THE JOURNAL OF PHYSICAL CHEMISTRY Letters

Letter

pubs.acs.org/JPCL

Entangled Valence Electron–Hole Dynamics Revealed by Stimulated Attosecond X-ray Raman Scattering

Daniel Healion,[†] Yu Zhang,[†] Jason D. Biggs,[†] Niranjan Govind,[‡] and Shaul Mukamel*[,†]

[†]Department of Chemistry, University of California, 450 Rowland Hall, Irvine, California 92697, United States

[‡]William R. Wiley Environmental Molecular Sciences Laboratory, Pacific Northwest National Laboratory, P.O. Box 999, Richland, Washington 99352, United States

Supporting Information

ABSTRACT: We show that broadband X-ray pulses can create wavepackets of valence electrons and holes localized in the vicinity of a selected atom (nitrogen, oxygen, or sulfur in cysteine) by stimulated resonant Raman scattering. The subsequent dynamics reveals highly correlated motions of entangled electron and hole quasiparticles. This information goes beyond the time-dependent total charge density derived from X-ray diffraction.

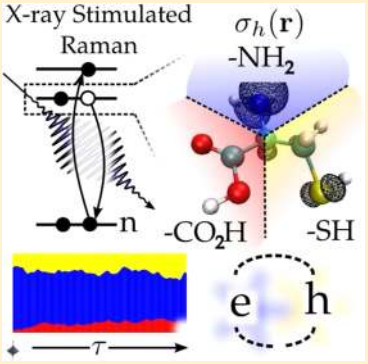

SECTION: Spectroscopy, Photochemistry, and Excited States

X-ray diffraction in crystals provides electron density maps that are widely used to determine high-resolution molecular structures. In this technique, hard X-ray photons scatter elastically off a static or time-dependent molecular charge density. There has been a steady effort to develop X-ray sources of ever increasing intensity[1,2] and shorter duration[3−7] that could be used for resonant, time-resolved spectroscopy of core electrons. Even though core-excited states are of fundamental interest, their high transition energies and short lifetimes (∼7.1 fs for nitrogen, ∼4.9 fs for oxygen,[8] and ∼1.1 fs for sulfur[9]) due to Auger decay make them less attractive targets for time-resolved experiments than the valence electronic states that directly participate in ordinary chemical processes. Attosecond resonant X-ray pulses, however, can be used to prepare valence excitations by a second-order inelastic stimulated Raman scattering. The evolution of these states reflects the dynamics of electron–hole excitations in the molecule. The idea draws on the analogy with the optical regime; some of the earliest applications of femtosecond pulses when they became available in the 1980s involved the preparation and monitoring of vibrational wavepackets.[10] Because of their broader bandwidth (fwhm 14.2 eV for a 128 as pulse), attosecond pulses can be similarly used to create and control wavepackets of valence electrons impulsively, providing a novel window into the chemical and optical properties of molecules. In the X-ray Raman technique, the core excitations merely serve as a fast trigger for the valence excitations in the same way that excited valence excitations act as a trigger for the slower vibrational motions in the optical regime.

Here we demonstrate the possible excitation selectivity offered by recently developed X-ray sources and how by preparing localized particle-hole excitations and monitoring their subsequent quantum evolution they can provide an unprecedented window into the many-body dynamics of valence excitations.

In a stimulated X-ray Raman process, a core electron is excited into an unoccupied virtual orbital for a very short time. A second valence electron is then stimulated to fill the core hole, resulting in a valence electron–hole pair.[11,12] The impulsive X-ray pulse creates a coherent superposition of such pairs, as allowed by its bandwidth. Shaping of the pulse envelopes can be used to further manipulate the wavepacket. The short core-hole lifetime is not a problem, provided the pulse is sufficiently intense and short.

A valence excitation initially localized to a selected atom can be created by tuning the X-ray pulse to be resonant with its core transition. The ground ($|g_o\rangle$), core-excited ($|e\rangle$), and valence excited ($|g'\rangle$) states of cysteine are calculated using restricted excitation window time-dependent density functional theory (REW-TDDFT)[13−16] implemented in a modified version of NWChem[17] (unpublished results). We focus on the purely electronic dynamics and neglect nuclear motions. This is justified for short time scales (<20 fs). The pulse

Received: July 18, 2012
Accepted: August 8, 2012
Published: August 8, 2012

prepares the molecule in a wavepacket of valence excited states $|g'\rangle$

$$|\psi(\tau)\rangle = \sum_{g'} \alpha_{g'g_o} e^{-i\varepsilon_{g'}\tau}|g'\rangle \quad (1)$$

Here α is the effective X-ray polarizability for the stimulated Raman process

$$\alpha_{j;g'g''} = \int_{\infty}^{\infty} \frac{(V_{g'e}\cdot V_{eg''})\mathcal{E}_j^*(\omega_2)\mathcal{E}_j(\omega_2 + \omega_{g'g''})}{\omega_2 + \omega_j - \omega_{eg'} + i\Gamma_e} d\omega_2 \quad (2)$$

where $\mathcal{E}_j(\omega)$ is the Fourier transform of the temporal envelope of the jth pulse, $V_{g'}$, $V_{eg''}$ are the dipole matrix elements, ω_j is the pulse central frequency, Γ_e is the lifetime decay of the core-excited state, and $\omega_{eg'} = \varepsilon_e - \varepsilon_{g'}$ is the energy difference between $|e\rangle$ and $|g'\rangle$.

A compact representation of the time-evolving state can be derived using superpositions of pairs of particle-hole natural orbitals[18,19]

$$|\psi(\tau)\rangle = \sum_{\xi=1}^{N} w_\xi(\tau) c_\xi^\dagger(\tau) d_\xi(\tau) \Big| g_o \Big\rangle \quad (3)$$

We define a creation operator $c_a^\dagger$ for an electron at the initially vacant valence orbital $\varphi_a(\mathbf{r})$, and an annihilation operator c_i for an electron from the occupied valence orbital $\varphi_i(\mathbf{r})$. $c_\xi^\dagger(\tau) = \sum_a V_{a,\xi}(\tau)c_a^\dagger$ and $d_\xi = \sum_i U_{i,\xi}{}^*(\tau)c_i$ represent corresponding operators for the natural orbitals ξ. The transformation matrices $V_{a,\xi}(\tau)$ and $U_{i,\xi}(\tau)$ as well as the coefficients $w_\xi(\tau)$ may be obtained by singular value decomposition[20] (SVD). These orbitals provide the most compact representation of the evolving state and therefore depend on time. Each $c_\xi^\dagger(\tau)d_\xi(\tau)$ operator creates a pair of particle (electron) $(c_\xi^\dagger)$ and hole (d_ξ) natural orbitals. The reduced electron and hole density matrix weights $w_\xi(\tau)$ are positive, and we use the normalization $\sum_\xi w_\xi^2(\tau) = 1$.

The net charge-density change measured by X-ray diffraction is the difference of the electron and hole densities. By revealing the electron and hole densities separately, stimulated Raman excitation contains signatures of their correlation and spatial coherence across the molecule; which are not otherwise available. Correlation-driven migration of an electron hole in the valence band of a molecule was simulated in previous studies[21−24] in which ultrafast hole motion was predicted. Those simulations assumed an initial, nonstationary state in which a core hole was prepared manually by simply removing an electron from a core orbital. Here we show how the entangled electron−hole state depends on the attosecond pulse envelope and further examine the dynamics of these coupled quasiparticles.

The spatial distribution of the particle (electron)

$$\sigma_p(\mathbf{r}) = \sum_\xi \left| \sum_a w_\xi(\tau) V_{\xi,a}(\tau)\phi_a(\mathbf{r}) \right|^2 \quad (4)$$

and the hole

$$\sigma_h(\mathbf{r}) = \sum_\xi \left| \sum_i w_\xi(\tau) U_{\xi,i}(\tau)\phi_i(\mathbf{r}) \right|^2 \quad (5)$$

created in the excited cysteine molecule after an X-ray excitation with a Gaussian pulse (fwhm 128 as; 14.2 eV) resonant with the N, O, or S K-edge are shown in Figure 1. At the nitrogen K-edge, the hole is localized on the nitrogen with

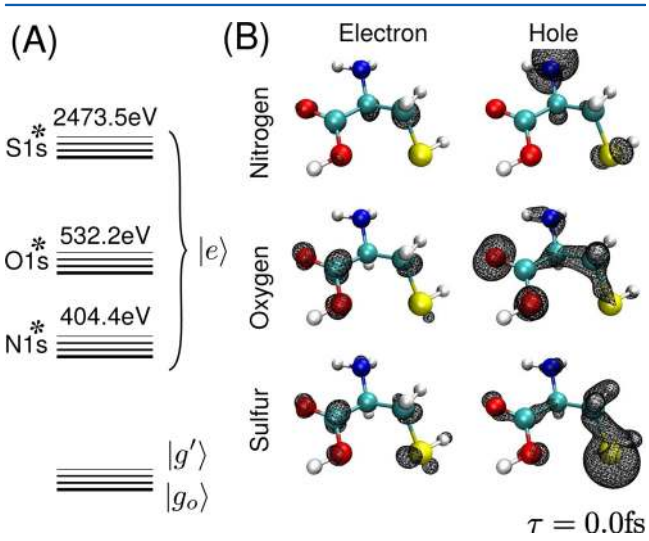

Figure 1. (A) Level scheme for the nitrogen (N1s*), oxygen (O1s*), and sulfur (N1s*) core-excited states at the K-edge. (B) Reduced electron and hole density contours $\sigma_{p,h}(\mathbf{r}) = 0.005$ au for a wavepacket directly after excitation with a pulse tuned to the nitrogen (top), oxygen (middle), and sulfur (bottom) K-edges.

little spread onto the neighboring carbon backbone; the particle is spread between the neighboring carboxyl and thiol groups. Excitation at the oxygen creates an electron with a strong π character local to the carboxyl group and a hole density distributed over σ-type excitations of the carboxyl and backbone. Sulfur excitation produces a particle and a hole with densities spread between the sulfur and the carboxyl group, with the hole showing a projection onto the σ-bond of the amide backbone. Several effects compete in creating these distributions. Selection rules in the K-edge X-ray Raman process favor final states with strong electron−hole projections onto the p orbitals of the resonant core atom. If the exciting pulse bandwidth is very broad, then the particle and hole should have mostly p-orbital excitation character. However, if transition densities with opposite phases on neighboring orbitals occur only at higher energies beyond the exciting pulse bandwidth, or no orbitals with significant projection onto the p-orbitals of the resonant core lie within the bandwidth of the pulse, then these particle or hole densities may be spread over neighboring atoms. Lower energy states should have a high probability for finding the electron on the electronegative carboxyl group and the hole on either the amine or thiol groups. By adjusting the exciting pulse to cover low energy states, we can select states with this preference.

A ∼25 fs movie of the time-evolution of the electron and hole densities following the Raman excitation is given in the Supporting Information. In all three cases, the electron resides preferentially on the carboxyl functional group. A few snapshots of the nitrogen K-edge excited density are shown in Figure 2. The electron probability distribution moves between the more electronegative carboxyl and thiol groups, whereas the hole created on the amine group remains there. To visualize the time-evolution of the density for each of the techniques, we have divided the nearly tetrahedral cysteine molecule into three regions containing the $-CO_2H$, $-NH_2$, and $-CH_2SH$ functional groups and integrated the reduced densities inside

dx.doi.org/10.1021/jz300981w | J. Phys. Chem. Lett. 2012, 3, 2326−2331

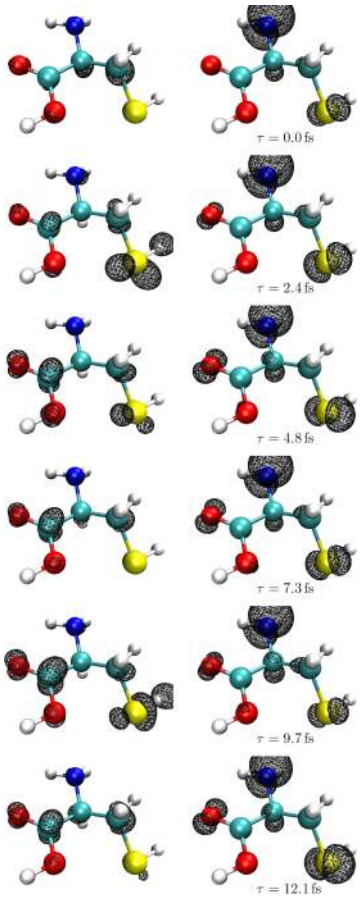

Figure 2. Six snapshots of the movie shown in the Supporting Information of the nitrogen-pumped wavepacket from $\tau = 0.0$ fs to $\tau \simeq 12$ fs.

these regions. This projection is depicted in Figure 3; details are given in the Supporting Information. The integrated intensity reveals the charge redistribution in the excited molecule. The particle densities are spread over the molecule, with the odds of finding the electron near the oxygen (39.5%) or sulfur (42.4%) after excitation at these groups slightly greater than those in the other regions of the molecule. The nitrogen particle has a smaller density (33.5%) on the amine group than on the carbon in the sulfur group (44.2%). The hole densities show a much stronger projection local to the resonant core: 78.8% for nitrogen, 45.4% for oxygen, and 69.6% for sulfur. From the subsequent evolution, we find that the hole created after excitation on the nitrogen remains on that functional group, whereas the holes and particles excited on oxygen and sulfur are more evenly delocalized between the three regions. By comparing the isosurface evolution for the electron probability after excitation at the nitrogen in Figure 2 with the integrated density in Figure 3, we see that at times the electron has an equal probability of being localized on either the amine or carboxyl; the isosurface encloses less area near the amine.

The Raman excited wavepackets contain a wealth of information regarding the correlated electron-hole motion that goes beyond their charge density alone. The natural orbital basis provides the most compact representation of electron−hole excitations. Both the number N of pairs included in the wavepacket and the natural orbital shapes themselves evolve with time. $N = 1$ signifies that the electrons and holes move independently and are uncorrelated; larger N indicates a higher degree of correlation.[25,26] Additional pulses tuned to be resonant with different atoms can further manipulate the electron−hole wavepacket. In the following simulations we applied two pulses separated by a delay $\tau = 24$ fs. There are nine possible combinations of two pulses each tuned to either the N, O, or S K-edges: N1s—O1s implies that the first pulse is tuned to the nitrogen edge, the second is tuned to oxygen, and

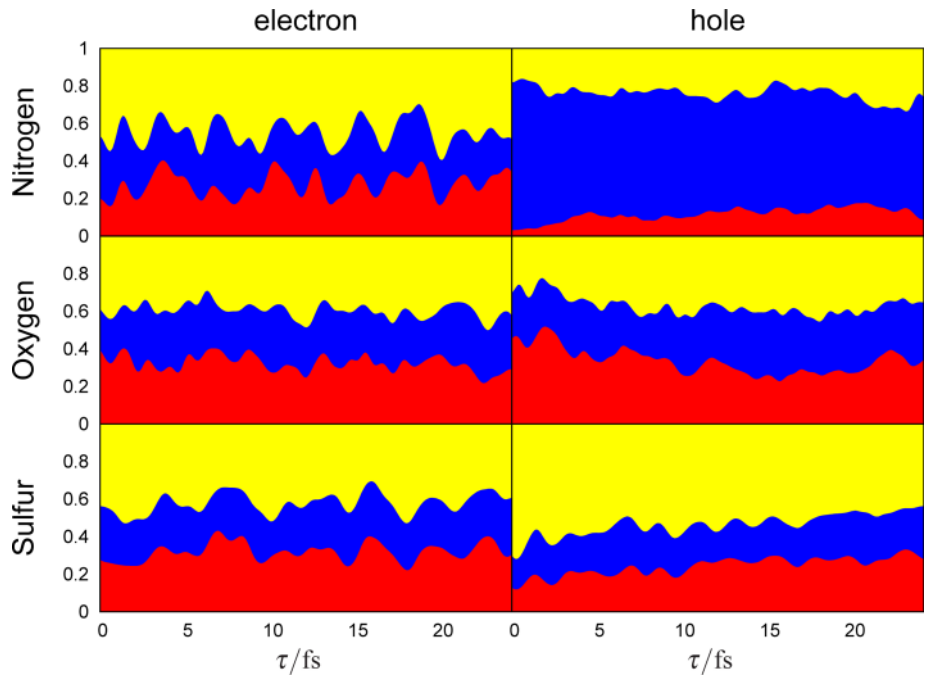

Figure 3. Distribution of the reduced electron (left column) and hole (right) densities over the carboxyl (red), amine (blue), and thiol (yellow) functional groups in cysteine after excitation with X-ray pulses tuned to the nitrogen (top row), oxygen (middle), and sulfur (bottom) K-edges. Computational details of this projection are given in the Supporting Information.

dx.doi.org/10.1021/jz300981w | J. Phys. Chem. Lett. 2012, 3, 2326−2331

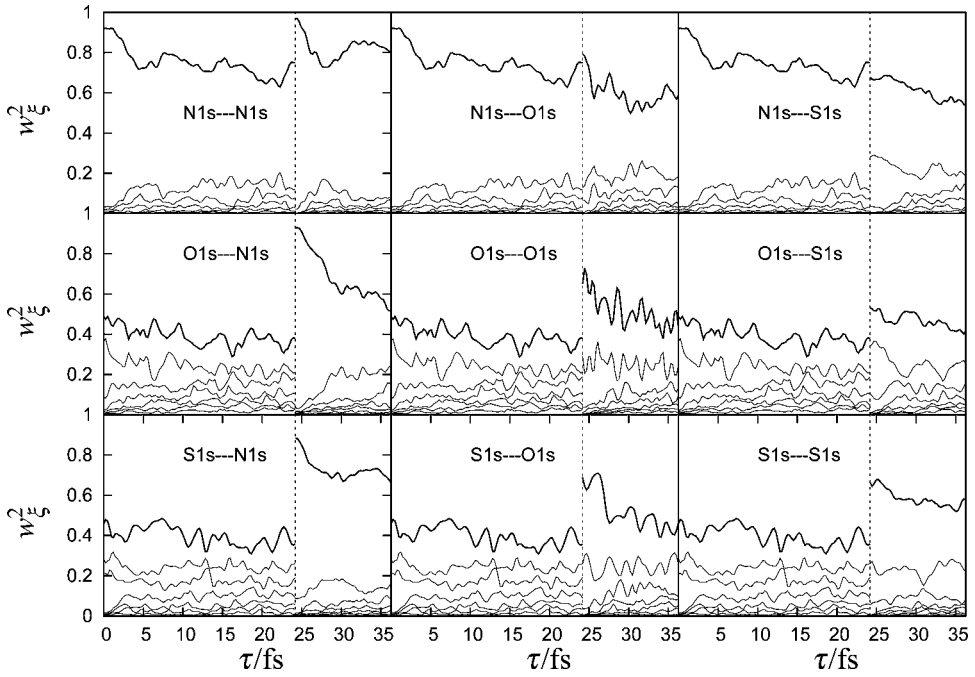

Figure 4. (top) Time variation of the normalized natural orbital SVD weights $w_\xi^2(\tau)$ for each particle-hole pair ξ with wavepackets created by pulses at $\tau = 0$, followed by a second pulse at $\tau = 24.2$ fs (dashed line). Each of these pulses can be tuned to be resonant with either the N, O, or S K-edges, giving rise to the nine scenarios, as indicated.

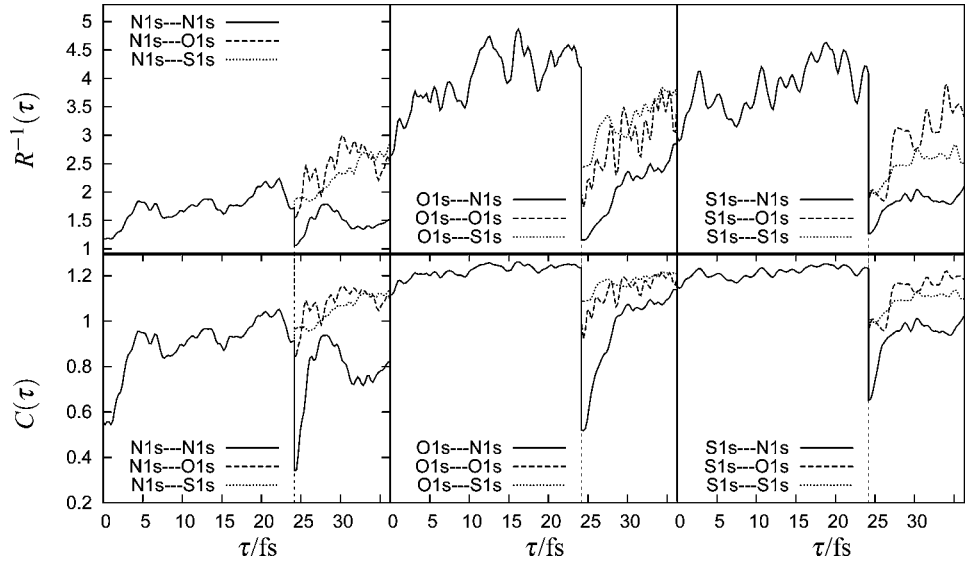

Figure 5. Measures of electron−hole entanglement: the time-dependent participation ratio $R^{-1}(\tau)$ (top) and the concurrence $C(\tau)$ (bottom). Notation and pulse sequence is as in Figure 4; the first pulse is tuned to the nitrogen (left), oxygen (middle), and sulfur (right) K-edge.

so forth. The squares of the time-dependent SVD weights $w_\xi^2(\tau)$ shown in Figure 4 reveal the multiparticle character of the entangled system. Initially the electron and hole are local to the resonant atom, and the time evolution of the natural orbitals reveals how they become delocalized with time. The many-body wavepacket involves several electron−hole pairs and represents a highly entangled state of these quasiparticles. For nitrogen excitation, the leading pair has 91% of the total weight, whereas for O and S it is only 49 and 46%, respectively. We have used two measures for the degree of entanglement between the bipartite electron and hole systems. The participation ratio

$$R^{-1}(\tau) = \frac{1}{\sum_\xi w_\xi^4(\tau)} \tag{6}$$

varies between 1 (uncorrelated electron−hole motion described by a single electron−hole product) and d, where d is the number of possible excitations in the basis. The concurrence

$$C(\tau) = \sqrt{2(1 - R(\tau))} \tag{7}$$

is another measure of entanglement commonly used in the field of quantum information[27] and varies between 0 (no entanglement) and $(2(d-1)/d)^{1/2}$.

The time evolution of both measures of entanglement are displayed in Figure 5. All panels show the relaxation from

dx.doi.org/10.1021/jz300981w | J. Phys. Chem. Lett. 2012, 3, 2326−2331

single- to many-excitation character of the wavepacket with time. Of the three resonant cores, nitrogen excitation has the least electron−hole entanglement during the first time-evolution period and the largest jump in the single-particle character when the second pulse is tuned to this transition, leading to the lowest participation ratio and concurrences. The N1s—O1s panel shows a marked increase in the participation ratios and concurrence after the second pulse relative to the N1s—S1s signal. The same trend is observed if the first pulse is tuned to sulfur (S1s—O1s and S1s—S1s) but not for the O1s—O1s and O1s—S1s configurations, which both have similar participation ratios for the second time-interval.

In summary, we have demonstrated the capacity of attosecond X-ray pulses to prepare electronic wavepackets with electron and hole densities local to the resonant core atom. These densities were calculated immediately after the excitation at the nitrogen, oxygen, and sulfur K-edges of cysteine, and movies of the time-evolving natural orbitals, the reduced electron and hole densities, and their degree of entanglement (natural orbital participation ratio and concurrence) illustrate the single particle character of the X-ray pulse and the subsequent dynamic many-body entanglement of quasiparticles. The time-dependent participation ratios show a rapid decay of the single particle-hole character of the excitation and the buildup of electron correlations in the valence excited states. Time-dependent particle hole occupations carry additional information on these correlations through both the reduced densities of the electrons and holes themselves and the cross-correlation between them. Identifying more detailed measures of these correlations and designing the optimal stimulated Raman, photoelectron, or other experimental techniques to measure this entanglement constitutes an interesting future challenge.

■ ASSOCIATED CONTENT

Supporting Information

Computational details, expressions for the Gaussian pulse-dressed X-ray polarizabilities, the particle and hole reduced density matrices, the angular projection scheme and an animated movie of the particle and hole densities in cysteine after excitation at the nitrogen, oxygen and sulfur K-edges. This material is available free of charge via the Internet at http://pubs.acs.org.

■ AUTHOR INFORMATION

Corresponding Author

*E-mail: smukamel@uci.edu.

Notes

The authors declare no competing financial interest.

■ ACKNOWLEDGMENTS

The support of the Chemical Sciences, Geosciences and Biosciences Division, Office of Basic Energy Sciences, Office of Science, U.S. Department of Energy is gratefully acknowledged. We also gratefully acknowledge the support of the National Science Foundation (Grant CHE-1058791), and the National Institutes of Health (Grant GM-59230). N.G. developed the restricted excitation window TDDFT (REW-TDDFT) in NWChem with support from EMSL at PNNL.

■ REFERENCES

(1) Emma, P.; et al. First Lasing and Operation of an Angstrom-Wavelength Free-Electron Laser. *Nat. Photon.* **2010**, *4*, 641−647.
(2) McNeil, B. W. J.; Thompson, N. R. X-ray Free-Electron Lasers. *Nat. Photon.* **2010**, *4*, 814−821.
(3) Krausz, F.; Ivanov, M. Attosecond Physics. *Rev. Mod. Phys.* **2009**, *81*, 163−234.
(4) Popmintchev, T.; Chen, M.; Arpin, P.; Murnane, M. M.; Kapteyn, H. C. The Attosecond Nonlinear Optics of Bright Coherent X-ray Generation. *Nat. Photon.* **2010**, *4*, 822−832.
(5) Li, W.; Zhou, X.; Lock, R.; Patchkovskii, S.; Stolow, A.; Kapteyn, H. C.; Murnane, M. M. Time-Resolved Dynamics in N_2O_4 Probed Using High-Harmonic Generation. *Science* **2008**, *322*, 1207−1211.
(6) Reiter, F.; et al. Route to Attosecond Nonlinear Spectroscopy. *Phys. Rev. Lett.* **2010**, *105*, 243902.
(7) Wörner, H. J.; Corkum, P. B. Attosecond Spectroscopy. In *Handbook of High-Resolution Spectroscopy*; Quack, M., Merkt, F., Eds.; John Wiley & Sons, Ltd.: Hoboken, NJ, 2011.
(8) Zschornack, G. H. *Handbook of X-ray Data*, 1st ed.; Springer: New York, 2007.
(9) Krause, M. O.; Oliver, J. H. Natural Widths of Atomic K and L levels, Kα X-ray Lines and Several KLL Auger Lines. *J. Phys. Chem. Ref. Data* **1979**, *8*, 329−338.
(10) Dhar, L.; Rogers, J. A.; Nelson, K. A. Time-Resolved Vibrational Spectroscopy in the Impulsive Limit. *Chem. Rev.* **1994**, *94*, 157−193.
(11) Biggs, J. D.; Zhang, Y.; Healion, D.; Mukamel, S. Two-Dimensional Stimulated Resonance Raman Spectroscopy of Molecules with Broadband X-ray Pulses. *J. Chem. Phys.* **2012**, *136*, 174117/1−174117/16.
(12) Schweigert, I. V.; Mukamel, S. Probing Valence Electronic Wave-Packet Dynamics by All Xray Stimulated Raman Spectroscopy: A Simulation Study. *Phys. Rev. A* **2007**, *76*, 012504/1−012504/9.
(13) Stener, M.; Fronzoni, G.; de Simone, M. Time Dependent Density Functional Theory of Core Electrons Excitations. *Chem. Phys. Lett.* **2003**, *373*, 115−123.
(14) Besley, N. A.; Noble, A. Time-Dependent Density Functional Theory Study of the X-ray Absorption Spectroscopy of Acetylene, Ethylene, and Benzene on Si(100). *J. Phys. Chem. C* **2007**, *111*, 3333−3340.
(15) DeBeer-George, S.; Petrenko, T.; Neese, F. Time-Dependent Density Functional Calculations of Ligand K-edge X-ray Absorption Spectra. *Inorg. Chim. Acta* **2008**, *361*, 965−972.
(16) Yanai, T.; Tew, D.; Handy, N. A New Hybrid Exchange Correlation Functional Using the Coulomb-Attenuating Method (CAM-B3LYP). *Chem. Phys. Lett.* **2004**, *393*, 51−57.
(17) Valiev, M.; Bylaska, E.; Govind, N.; Kowalski, K.; Straatsma, T.; van Dam, H.; Wang, D.; Nieplocha, J.; Apra, E.; Windus, T.; et al. NWChem: A Comprehensive and Scalable Open-Source Solution for Large Scale Molecular Simulations. *Comput. Phys. Commun.* **2010**, *181*, 1477−1489.
(18) Amos, A. T.; Hall, G. G. Single Determinant Wave Functions. *Proc. R. Soc. London, Ser. A* **1961**, *263*, 483−493.
(19) Martin, R. L. Natural Transition Orbitals. *J. Chem. Phys.* **2003**, *118*, 4775−4777.
(20) Golub, G. H.; Van Loan, C. F. *Matrix Computations*, 3rd ed.; Johns Hopkins Studies in Mathematical Sciences; The Johns Hopkins University Press: Baltimore, 1996.
(21) Breidbach, J.; Cederbaum, L. S. Migration of Holes: Formalism, Mechanisms, and Illustrative Applications. *J. Chem. Phys.* **2003**, *118*, 3983−3996.
(22) Breidbach, J.; Cederbaum, L. S. Migration of Holes: Numerical Algorithms and Implementation. *J. Chem. Phys.* **2007**, *126*, 034101/1−034101/15.
(23) Kuleff, A. I.; Cederbaum, L. S. Tracing Ultrafast Interatomic Electronic Decay Processes in Real Time and Space. *Phys. Rev. Lett.* **2007**, *98*, 083201/1−083201/4.
(24) Kuleff, A. I.; Breidbach, J.; Cederbaum, L. S. Multielectron Wave-Packet Propagation: General Theory and Application. *J. Chem. Phys.* **2005**, *123*, 044111/1−044111/10.

(25) Mintert, F.; Carvalho, A. R.; Kus, M.; Buchleitner, A. Measures and Dynamics of Entangled States. *Phys. Rep.* **2005**, *415*, 207−259.
(26) Mukamel, S.; Wang, H. Manipulating Quantum Entanglement of Quasiparticles in Many-Electron Systems by Attosecond X-ray Pulses. *Phys. Rev. A* **2010**, *81*, 062334/1−062334/4.
(27) Hill, S.; Wootters, W. K. Entanglement of a Pair of Quantum Bits. *Phys. Rev. Lett.* **1997**, *78*, 5022−5025.